Mechanisms of Cx43 and Cx26 transport to the plasma membrane and gap junction regeneration

Tamsin Thomas, Karen Jordan, Jamie Simek, Qing Shao, Chris Jedeszko, Paul Walton and Dale W. Laird*

Department of Anatomy and Cell Biology, University of Western Ontario, Dental Science Building, Rm. 00077, London, Ontario, Canada N6A 5C1

*Author for correspondence (e-mail: dale.laird@fmd.uwo.ca)

Accepted 5 July 2005
Journal of Cell Science 118, 4451-4462 Published by The Company of Biologists 2005
doi:10.1242/jcs.02569

Summary

Previous reports have suggested that Cx26 exhibits unique intracellular transport pathways en route to the cell surface compared with other members of the connexin family. To directly examine and compare nascent and steady-state delivery of Cx43 and Cx26 to the plasma membrane and gap junction biogenesis we expressed fluorescent-protein-tagged Cx43 and Cx26 in BICR-M1R$_k$ and NRK cells. Static and time-lapse imaging revealed that both connexins were routed through the Golgi apparatus prior to being transported to the cell surface, a process inhibited in the presence of brefeldin A (BFA) or the expression of a dominant-negative form of Sar1 GTPase. During recovery from BFA, time-lapse imaging of nascent connexin Golgi-to-plasma membrane delivery revealed many dynamic post-Golgi carriers (PGCs) originating from the distal side of the Golgi apparatus consisting of heterogeneous vesicles and long, tubular-like extensions. Vesicles and tubular extensions were also observed in HBL-100 cells expressing a human, disease-linked, Golgi-localized Cx26 mutant, D66H-GFP. A diffuse cell surface rim of fluorescent-protein-tagged wild-type connexins was observed prior to the appearance of punctate gap junctions, which suggests that random fusion of PGCs occurred with the plasma membrane followed by lateral diffusion of connexins into clusters. Fluorescence recovery after photobleaching studies revealed that Cx26-YFP was more mobile within gap junction plaques compared with Cx43-GFP. Intriguingly, Cx43-GFP delivery and gap junction regeneration was inhibited by BFA and nocodazole, whereas Cx26-GFP delivery was prevented by BFA but not nocodazole. Collectively, these studies suggest that during gap junction biogenesis two phylogenetically distinct members of the connexin family, Cx43 and Cx26, share common secretory pathways, types of transport intermediates and turnover dynamics but differ in their microtubule-dependence and mobility within the plasma membrane, which might reflect differences in binding to protein scaffolds.

Supplementary material available online at
http://jcs.biologists.org/cgi/content/full/118/19/4451/DC1

Key words: Connexin, Gap junctions, Post-Golgi carriers, Time-lapse imaging, Fluorescence recovery after photobleaching

Introduction

Gap junctions are specialized intercellular channels that allow for the direct transfer of small signaling and regulatory molecules between contacting cells (Saez et al., 2003). The protein subunits of gap junctions are encoded by the connexin (Cx) gene family and six connexin proteins oligomerize into a hexameric structure called a connexon or hemichannel. Connexons are transported to the plasma membrane and pair with connexons from contacting cells to form gap junction channels (Saez et al., 2003). When channels cluster at the cell surface into tightly packed arrays, they form a gap junction or gap junction plaque (Saez et al., 2003). Many cell types and tissues are known to express more than one of the 20 members of the connexin family (Willecke et al., 2002) and all connexins share common characteristics in regard to their topology and channel forming ability (Saez et al., 2003).

Connexins are co-translationally inserted into the endoplasmic reticulum (ER), although cell-free studies revealed that Cx26 and Cx43 can also post-translationally insert into ER membranes (Ahmad et al., 1999; Zhang et al., 1996), and one report suggests that Cx26 can even directly insert into plasma membranes (Ahmad and Evans, 2002). It is well documented that Cx43 and Cx46 oligomerize into connexons in compartments that include the TGN (Koval et al., 1997; Musil and Goodenough, 1993), while others have found evidence that supports Cx32 and Cx26 oligomerization occurring primarily within ER membranes (Falk et al., 1997; Falk and Gilula, 1998; Falk et al., 1994). Additional studies in which aequorin- or GFP-tagged Cx26 trafficking exhibited insensitivity to brefeldin A (BFA) suggested that Cx26 may bypass the Golgi apparatus en route to the cell surface (Evans et al., 1999; George et al., 1999; George et al., 1998b; Martin et al., 2001). These same studies also reported that Cx26 transport was sensitive to nocodazole whereas Cx32 and Cx43 transport were not. Consequently, it has been proposed that Cx26 has transport and assembly properties that are distinct from other connexins. Additionally, fluorescent-protein-tagged Cx43 and Cx26 were found to both segregate into sub-domains and intermix within the same gap junction plaques (Falk, 2000). Furthermore, Cx43 and Cx26 do not form heteromeric connexons (Gemel et al., 2004), which reflects possible distinct differences in the assembly of connexin isotypes. Nevertheless,

studies from disease-causing human Cx26 mutants have revealed a steady-state reservoir of Cx26 within the trans-Golgi network (Thomas et al., 2004) similar to Cx43 (Laird et al., 1995). This collection of studies has resulted in considerable debate as to how Cx26 is transported within mammalian cells during gap junction biogenesis. The importance of this debate has been elevated in recent years as it appears that the manifestation of human deafness in combination with etiologies of epidermal keratodermas depends extensively on the trans-dominant interactions of Cx26 mutants with other members of the connexin family (Bakirtzis et al., 2003; Forge et al., 2003; Marziano et al., 2003; Rouan et al., 2001; Thomas et al., 2004), possibly by co-oligomerization of the mutant with wild-type connexins while they co-reside within the same intracellular compartments. Likewise, the recent identification of Cx43 point mutations linked to oculodentodigital dysplasia (ODDD) (Paznekas et al., 2003; Richardson et al., 2004) has raised similar questions as to how Cx43 mutants may crosstalk with other members of the connexin family, including Cx26.

To date, limited studies have investigated the types of transport intermediates that deliver connexins to the cell surface and the dynamic processes of gap junction plaque assembly in live cells. In the present study, we chose to compare and contrast the types of transport intermediates and the process of delivery of GFP-tagged Cx43- and Cx26-containing post-Golgi carriers (PGCs) during nascent and steady-state gap junction assembly in live BICR-M1R_k and NRK cells.

Materials and Methods

Cells and reagents

All media, sera and reagents were obtained from Invitrogen (Burlington, ON, Canada), BD Biosciences (Mississauga, ON, Canada) or Sigma-Aldrich Canada (Oakville, ON, Canada). Lipofectamine Plus and Lipofectamine 2000 reagents were obtained from Invitrogen. Normal rat kidney cells (NRK-52E) (American Type Culture Collection, Rockville, MD; 1571-CRL), BICR-M1R_k cells, derived from a rat mammary tumor (Laird et al., 1995), and HBL-100 cells (Qin et al., 2001) were grown in DMEM supplemented with 10% fetal bovine serum, 100 U/ml penicillin, 100 μg/ml streptomycin and 2 mM glutamine. Brefeldin A (BFA) and nocodazole were purchased from Sigma.

DNA, transfections and generation of stable cell lines

Engineering of the Cx43-green fluorescent protein (Cx43-GFP) was as described previously (Jordon et al., 1999). The Cx26-YFP plasmid was designed as previously described (Laird et al., 2001). Cx26-GFP and Cx26 mutants D66H-GFP and D66K-GFP were prepared as described (Thomas et al., 2004). For preparation of wild-type human Sar1 cDNA, total RNA from a human fibroblast cell line (Hs27) was isolated using Trizol (Invitrogen). RT-PCR was performed with the Superscript III One-Step RT-PCR System with Platium *Taq* DNA Polymerase (Invitrogen). The following primer set was used to amplify Sar1 cDNA: Forward 5′-GATAAGCGCTATGTCTTTCATC-TTTGAGTGG-3′, Reverse 5′-GCTCGAATTCTCAGTCAATATA-CTGGGAGAG-3′. The GTP-restricted amino acid mutation H79G was generated by site-directed mutagenesis using the QuikChange Site-Directed Mutagenesis Kit from Stratagene (La Jolla, CA) as directed. The mutagenesis primer sets were as follows: Forward 5′-CTTTTGATCTTGGTGGGGGCGAGCAAGCACGTCGCG-3′ and Reverse 5′-CGCGACGTGCTTGCTCGCCCCCACCAAGATCAA-AAG-3′. The mutated nucleotides are underlined. Wild-type and mutated Sar1 cDNAs were amplified by PCR (using *Pfu* polymerase from Fermentas, Burlington, ON, Canada) with primers designed to add restriction enzymes sites for *Xho*I and *Eco*RI and to remove the stop codon so that Sar1- or mutSar1-DsRed2 fusion proteins could be developed. Following PCR, Sar1 and mutSar1 cDNAs were cloned into the *Xho*I and *Eco*RI sites of pDsRed2-N1 (Clontech, Palo Alto, CA).

For transient transfections of Cx43-GFP, Sar1-DsRed2 or mutant Sar1-DsRed2, BICR-M1R_k cells were plated on glass coverslips and grown to 50-75% confluence overnight in 35 mm or 60 mm culture dishes or in 35 mm glass-bottom tissue culture dishes (MatTek Corporation, MA). BICR-M1R_k cells were transfected using Lipofectamine PLUS as described (Jordan, et al., 1999) with 1 μg of Cx43-GFP plasmid DNA. In other cases we used 4 μl of Lipofectamine 2000 and 2 μg of Sar1-DsRed2 or mutSar1-DsRed2 plasmid DNA per 35 mm glass-bottom tissue culture dish. Cells were then prepared for immunolabeling or for time-lapse imaging as described below. Retroviral infection of NRK, BICR-M1R_k, or HBL-100 cells with cDNA encoding Cx26, Cx43-GFP, Cx26-YFP, Cx26-GFP, D66H-GFP or D66K-GFP within the AP2 retroviral vector (Galipeau et al., 1999) was performed as described (Mao et al., 2000; Qin et al., 2002; Thomas et al., 2004). Thus, the majority of the data presented herein were obtained from cell lines stably expressing various connexins or Cx-GFPs. Only the images of BICR-M1R_k cells expressing Cx43-GFP in Fig. 5A1,A2 and B, and the corresponding time-lapse images, as well as the expression of Sar1-DsRed2 or mutSar1-DsRed2 were transient transfections.

Drug treatments: BFA and nocodazole

To analyze ER-to-Golgi connexin transport, BICR-M1R_k cells expressing the appropriate connexins were treated for 6 hours with BFA (5 μg/ml). BFA was removed from the culture medium by washing cells three times with regular growth medium and incubating for 0, 30, 60, 90 and 120 minutes after BFA removal. In the case of FRAP of NRK cells expressing fluorescent-protein-tagged Cx43 or Cx26, cells were pre-treated with 5 μg/ml BFA for 45 minutes and assessed by time-lapse imaging. To analyze the role of microtubules in vesicular connexin transport, NRK cells expressing fluorescent-protein-tagged Cx43 or Cx26 were first time-lapse imaged (32 second image acquisition intervals) for up to 18 minutes. After treating the cells for 45 minutes with nocodazole (10 μM) to disrupt the microtubules (Thomas et al., 2001), the same field of cells was again time-lapse imaged over an additional period of up to 18 minutes. LSM 510 software was used to calculate the individual vesicle displacement over 1 minute from time-lapse images of cells before and after microtubule disruption as modified from the procedure described previously (Johnson et al., 2002). The movement of 20 randomly chosen vesicles was measured from each of three independent experiments and the results reported as the average vesicle displacement ± standard error. This analysis was performed by two investigators who were blinded to the treatment condition. Note that only vesicles that remained in z-focus from one time frame to the next were quantified. Finally, the Student's unpaired *t*-test was performed using GraphPad Prism version 4.00 for Windows (GraphPad Software, San Diego, CA) to compare the vesicle movement from control and nocodazole-treated cells.

In other experiments, gap junctions of untreated cells or cells pre-treated with 10 μM nocodazole for 45 minutes were subjected to FRAP analysis. Additionally, microinjection of untreated or BFA-treated (6 hours), Cx26-expressing BICR-M1R_k cells with 5% Lucifer Yellow was carried out as described previously (Thomas et al., 2004).

Immunocytochemistry

Cells were immunolabeled as previously described (Laird et al., 1995). A mouse anti-Cx43 monoclonal antibody was purchased from

Chemicon International (Temecula, CA) and a polyclonal anti-Cx43 antibody was obtained from Sigma. Mouse anti-Cx26 antibodies were obtained from Zymed (San Francisco, CA) and Cx26IL-1 antibody was acquired from the Fred Hutchinson Cancer Research Center Antibody Development Group. The rabbit polyclonal antibody specific for a medial Golgi protein, MG160, was a generous gift from N. Gonatas (The University of Pennsylvania, Philadelphia, PA) (Gonatas et al., 1989). Finally, the polyclonal GPP130 antibody (medial Golgi apparatus protein) was purchased from Covance Research Products (Berkeley, CA). Secondary antibodies included goat anti-mouse or donkey anti-rabbit antibodies conjugated to Texas Red, AMCA or FITC (Jackson ImmunoResearch, West Grove, PA). Fluorescent samples were analyzed on a Zeiss (Thornwood, NY) LSM 410 inverted confocal microscope as previously described (Laird et al., 1995) or a Zeiss LSM 510 META confocal microscope. GFP, YFP or FITC were excited using a 488 nm argon laser line and emissions collected after light passage through a 500-550 nm band pass filter. Texas Red or DsRed2 was excited using the 543 nm helium-neon laser line and emissions collected between 600-650 nm (tunable channel). AMCA was excited using a Chameleon multi-photon laser with the excitation wavelength set to 720 nm and emissions were collected after passage through a 400-450 nm band pass filter. The multi-track setting was used to further minimize any potential bleed through of GFP, YFP or FITC signals into red channels.

Live cell connexin transport assays in BICR-M1R$_k$ cells

BICR-M1R$_k$ cells transiently expressing Cx43-GFP or stably expressing Cx26-YFP were plated in 35 mm glass-bottom tissue culture dishes for live imaging (MatTek Corporation, MA). For live cell imaging, culture medium containing BFA was replaced with 2 ml of Hank's balanced salt solution supplemented with 2 mM glutamine, 100 U/ml penicillin, 100 μg/ml streptomycin, 200 μg/ml calcium chloride and 100 μg/ml magnesium sulfate, with either 10 mM Hepes buffer, pH 7.2, or OptiMEM-I (reagents purchased from Gibco BRL or Sigma Chemical Company). Live cells were placed on a 20/20 Technology (Mississauga, ON, Canada) temperature-controlled stage that maintained cells at 37°C for the duration of live cell imaging during recovery from BFA treatment. Cells were time-lapse imaged on a Zeiss LSM 410 confocal microscope 10 minutes–2.25 hours after the removal of BFA. Cx43-GFP or Cx26-YFP was excited with a 488 nm argon/krypton laser line and images were collected using a 63× lens after fluorescent light passage through a 500-550 nm band pass filter. Optical sections were line-scanned continuously at a scan speed of 32 seconds/image and collected for periods of up to 50 minutes. The size of the tubular-shaped post-Golgi carriers (PGCs) containing Cx43-GFP and Cx26-YFP were calculated using the measure function macro within the LSM 410 software. All focus, contrast and brightness settings remained constant during imaging acquisition. Time-lapse images were animated using Adobe Premiere software.

Fluorescent recovery after photobleaching (FRAP) analysis of gap junction regeneration

FRAP was performed on a Zeiss LSM 510 META microscope using the 'Edit Bleach' function in combination with 'Time Series' LSM 510 software. A region of interest was chosen and 100-150 iterations of the 488 nm laser line at 100% emission strength were used to completely photobleach the fluorescence within the region of interest. The progression of FRAP was followed by continuously acquiring 4 second images with a time interval of 30 seconds for up to 2 hours of total imaging time. The microscope was equipped with an environmental chamber (Incubator S) with CO_2 controller so that cells were maintained in regular growth medium at 37°C and 5% CO_2. The pinhole was set so that 2 μm optical slices were collected. FRAP of HBL-100 cells expressing Golgi-retained D66H-GFP or D66K-GFP was carried out similarly. For FRAP within individual gap junction plaques composed of Cx26-YFP or Cx43-GFP in BICR-M1R$_k$ cells, 40-60 iterations of the 488 nm laser line at 100% emission strength was used to photobleach the regions of interest

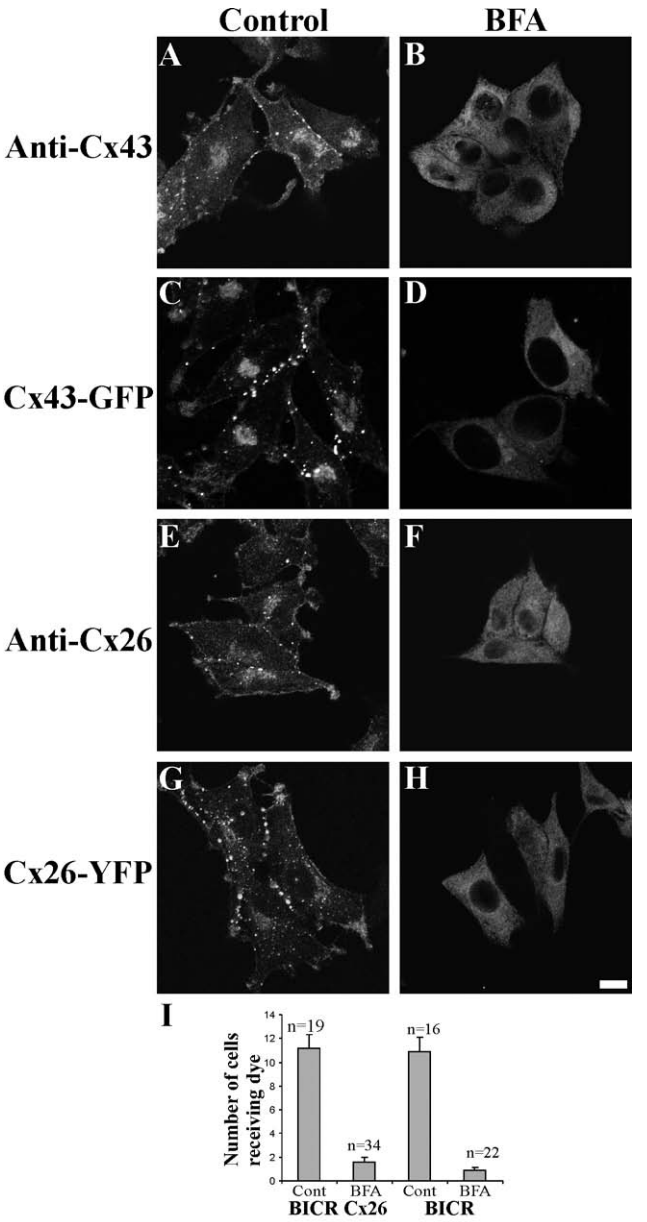

Fig. 1. BICR-M1R$_k$ cells assemble untagged and fluorescent-protein-tagged Cx26 and Cx43 into gap junctions via a trafficking pathway that is BFA-sensitive. Wild-type BICR-M1R$_k$ (A,B) or BICR-M1R$_k$ stably expressing Cx43-GFP (C,D), Cx26 (E,F) or Cx26-YFP (G,H) were immunolabeled for either Cx43 (A,B) or Cx26 (E,F); fluorescent-protein-tagged connexins were imaged without further processing. There was a prominent untagged or fluorescent-protein-tagged paranuclear-localized and plasma membrane-localized connexin population in untreated cells (A,C,E,G). However, following BFA treatment, all connexin variants were localized in an ER-like pattern (B,D,F,H) and gap junction plaques were not evident. Bar, 10 μm. (I) BFA-treatment of cells co-expressing Cx43 and Cx26 (BICR Cx26) dramatically inhibited dye coupling. Data expressed as mean number of cells receiving dye before or after BFA treatment±s.e.m.

(ROI). A scan was acquired every second during recovery from photobleaching. Fluorescence recovery of the mobile fraction was quantified using the 'Mean ROI' function within the Zeiss LSM 510 META software package. Fluorescence intensities of ROIs were recorded at the following time periods: prior to photobleaching (pre-bleach), immediately after photobleaching (t=0 seconds), and at 25, 50, 100, 150, 200 and 300 seconds post-bleach. Post-bleach intensities were corrected for any residual, non-bleached fluorescence, as described by previously (Lippincott-Schwartz et al., 2001). Averages were taken at each time point and the data plotted using GraphPad Prism version 4.00 for Windows (GraphPad Software, San Diego, CA). Finally, a non linear regression was used to create a best fit curve.

Results

Transport of untagged and fluorescent-protein-tagged Cx43 and Cx26 to the cell surface requires functional ER-to-Golgi delivery

We previously showed that fluorescent-protein-tagged Cx26 is functional as assessed by dye transfer studies (Thomas et al., 2004). Likewise, we established that Cx43-GFP localizes to the Golgi apparatus, was efficiently transported to the cell surface and was assembled into gap junctions at the plasma membrane (Jordan et al., 1999). In order to further validate the use of GFP-tagged Cx43 in live cell studies, we showed that, in BICR-M1R$_k$ cells, endogenous Cx43 and GFP-tagged Cx43 have comparable intracellular and cell membrane localization patterns and are assembled into similar-sized gap junctions (Fig. 1A,C). Likewise, when untagged or YFP-tagged Cx26 was expressed in BICR-M1R$_k$ cells, both molecules assembled into spatially similar gap junctions (Fig. 1E,G). We previously showed that BICR-M1R$_k$ cells efficiently remove Cx43-containing gap junction plaques from the cell surface within 6 hours of treatment with the protein trafficking inhibitor, BFA and, importantly, nascent gap junction plaque assembly can be followed upon the removal of BFA (Laird et al., 1995). Following 6 hours of BFA treatment, Cx43, Cx43-GFP, Cx26 and Cx26-YFP all exhibited an ER-like localization pattern with an absence of detectable gap junction plaques (Fig. 1B,D,F,H). Consistent with the loss of gap junction plaques, when BFA-treated BICR-M1R$_k$ cells (express endogenous Cx43) or BICR-M1R$_k$ cells that express Cx26 were microinjected with Lucifer Yellow, dye coupling was inhibited by over 80% (Fig. 1I).

Cx26 transport to the cell surface is inhibited by expression of a dominant-negative Sar1 mutant

We further tested the necessity of functional ER-to-Golgi protein trafficking for both Cx43 and Cx26 delivery to the cell surface by engineering BICR-M1R$_k$ cell lines that stably express Cx26, Cx26-YFP or Cx43-GFP to co-express wild-type Sar1-DsRed2 or a GTP-restricted mutant form (H79G) of Sar1-DsRed2. Sar1 (secretion-associated and Ras-related) is a small GTPase that controls the assembly of COPII protein coats to direct vesicle budding from the ER (Haucke, 2003). Mutation of Sar1 into the GDP- or GTP-restricted form inhibits the budding of COPII-dependent vesicles from the ER (Aridor et al., 1995; Dascher and Balch, 1994) and hence blocks the classical secretory pathway. We first verified that mutSar1-DsRed2 inhibited ER-to-Golgi-protein traffic by localizing the resident Golgi protein GPP130 in BICR-M1R$_k$ cells transfected with Sar1-DsRed2 or mutSar1-DsRed2 (Fig. 2A-F). Expression of wild-type Sar1-DsRed2 did not affect the distribution of

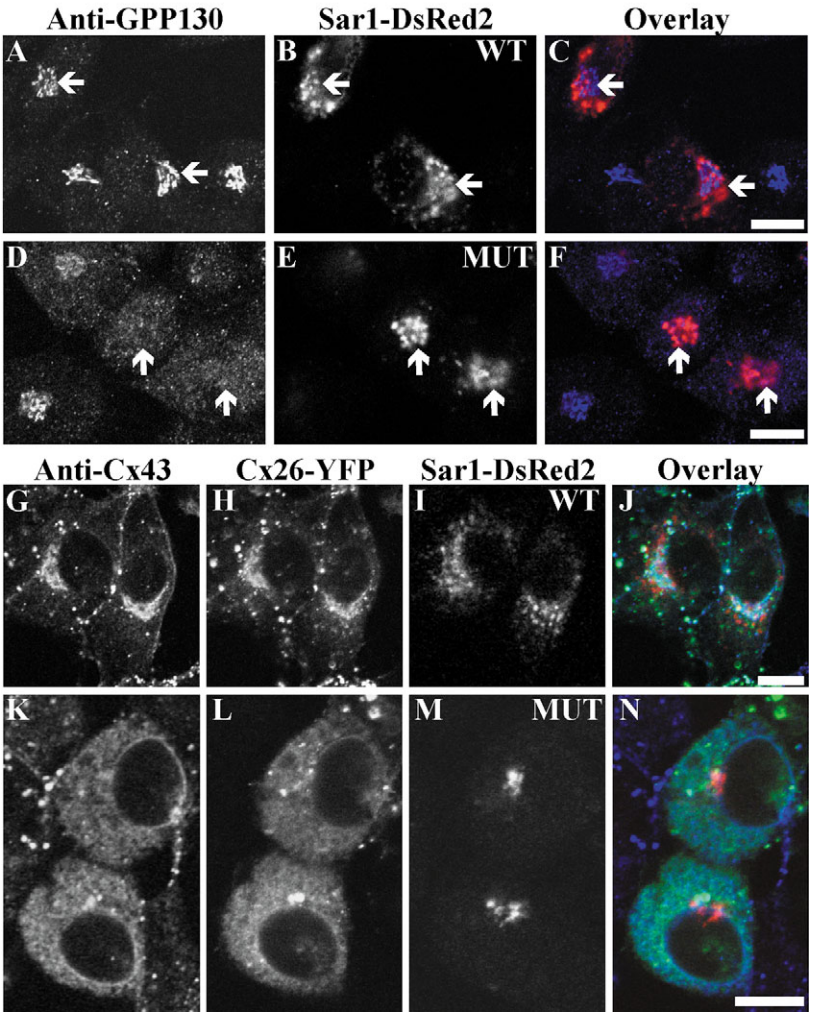

Fig. 2. Expression of mutant Sar1 disrupts ER-to-Golgi transport in BICR-M1R$_k$ cells and inhibits Cx26 and Cx43 trafficking to the cell surface. BICR-M1R$_k$ cells were transiently transfected with either Sar1-DsRed2 (A-C) or mutSar1-DsRed2 (D-F), and immunolabeled for the Golgi-resident protein GPP130 (A,D). The Golgi apparatus, as defined by GPP130 localization (arrows), remained intact in the presence of Sar1-DsRed2 but was disrupted in cells expressing mutSar1-DsRed2. BICR-M1R$_k$ cells stably expressing Cx26-YFP were transiently transfected with Sar1-DsRed2 (G-J) or mutSar1-DsRed2 (K-N) and immunolabeled for Cx43. Anti-rabbit AMCA was used to visualize and separate the Cx43 signal from YFP and DsRed fluorescence. Sar1-DsRed2 did not disrupt the localization pattern of Cx43 or Cx26-YFP but mutSar1-DsRed2 caused their retention within the ER. Bars, 10 μm. WT, wild-type; MUT, mutant.

GPP130 (Fig. 2A-C, arrows), whereas mutSar1-DsRed2 led to the loss of paranuclear GPP130 (Fig. 2D-F, arrows). BICR-M1R$_k$ cells co-expressing endogenous Cx43, Cx26-YFP and Sar1-DsRed2 revealed typical Cx43/Cx26 gap junction plaques at intercellular interfaces as well as paranuclear-localized (i.e. Golgi-localized) Cx43 and Cx26 (Fig. 2G-J). Upon expression of mutSar1-DsRed2, both Cx43 and Cx26-YFP exhibited an ER-like pattern (Fig. 2K-N). The punctate structures remaining in Fig. 2K were from a neighboring, non-transfected cell. These results reveal that both Cx43 and Cx26 transport beyond the ER requires functionally competent Sar1.

Connexin routing and transport intermediates involved in nascent gap junction plaque assembly

Since both Cx43 and Cx26 transport to the cell surface were found to be BFA-sensitive and gap junction plaques composed of either connexin could be cleared from the cell surface in the presence of BFA, we examined the kinetics, transport intermediates and connexin routing during nascent gap junction plaque formation (Fig. 3). In this case, BICR-M1R$_k$ cells that co-express endogenous Cx43 and untagged Cx26 were treated with BFA for 6 hours and the transport and assembly of both connexins were examined simultaneously after BFA wash-out. In untreated cells, Cx26 and Cx43 co-localized within gap junction plaques at the cell surface (Fig. 3A-C, arrows), as well as within paranuclear structures representing the Golgi apparatus (Fig. 3A-C, double arrows). After BFA treatment, Cx26 and Cx43 were both localized in reticular structures reminiscent of the ER (Fig. 3D-F). After BFA was removed for 30 minutes, a subpopulation of both Cx43 and Cx26 was localized to the reforming Golgi apparatus (Fig. 3G-I, double arrows). After 90 minutes, both Cx43 and Cx26 were enriched in the Golgi apparatus (Fig. 3J-L, double arrows), there was a diffuse population of both Cx43 and Cx26 surrounding the whole cell, including non-cell-cell interfaces (Fig. 3J-L, arrow), and gap junction plaques were beginning to form at cell-cell interfaces (Fig. 3J-L, arrowhead). Finally, after 2 hours of recovery from BFA treatment, the cells appeared to reach a steady-state where gap junction plaques and a Golgi pool of both Cx43 and Cx26 were evident, which resembled untreated cells (Fig. 3M-O).

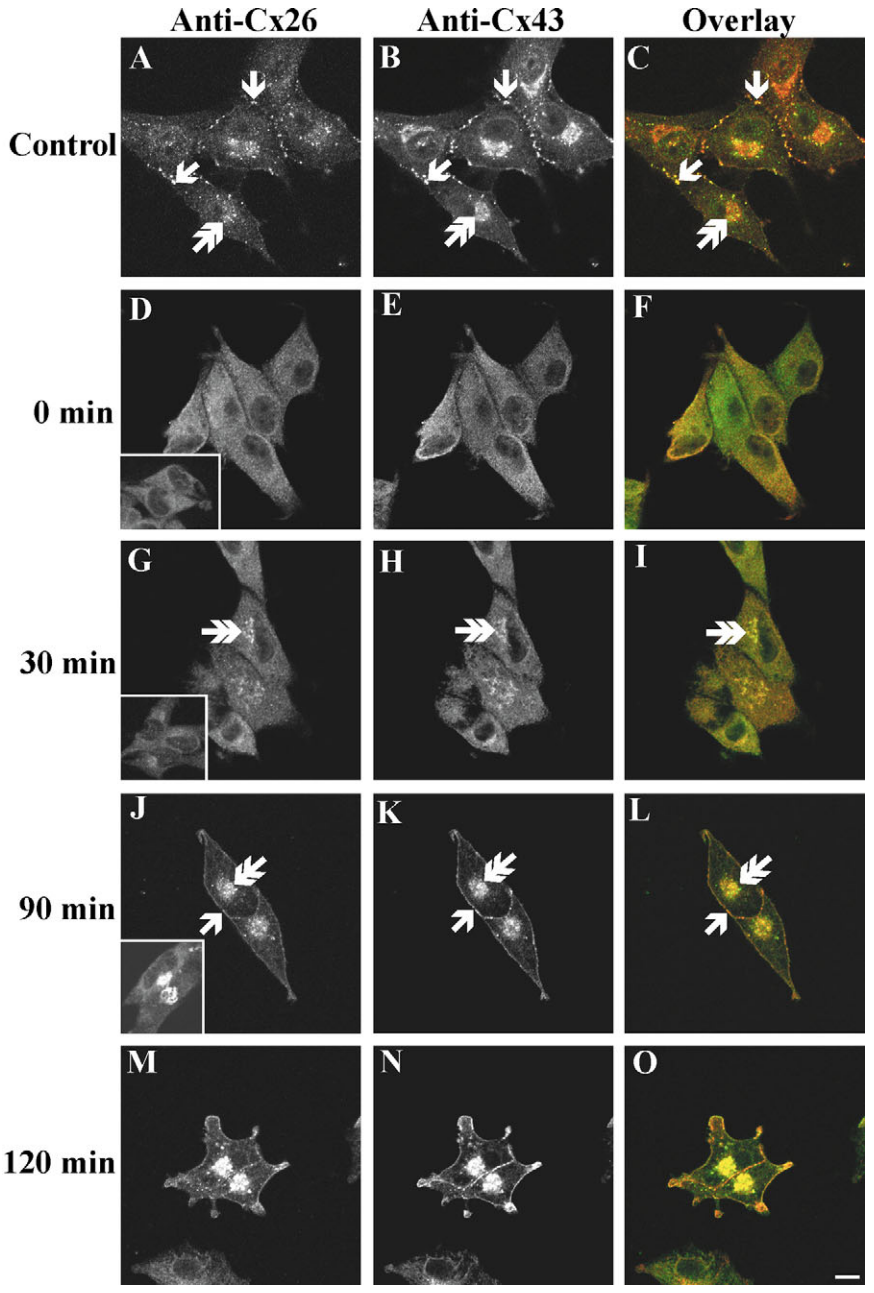

Fig. 3. Cx26 and Cx43 exhibit similar kinetics and follow identical pathways during nascent gap junction biogenesis. BICR-M1R$_k$ cells stably expressing Cx26 were treated with BFA for 6 hours and fixed at different times following BFA-washout prior to double immunofluorescently labeling for Cx26 (A,D,G,J,M; green) or Cx43 (B,E,H,K,N; red). In untreated conditions, Cx26 and Cx43 often co-localized to the same gap junctions (A-C, arrows) and within paranuclear regions of the cells consistent with localization to the Golgi apparatus (A-C, double arrows). Immediately after BFA removal, Cx26 and Cx43 exhibited an ER-like localization pattern (D-F; inset in D reveals a similar distribution of the resident Golgi protein, MG160). At 30 minutes post-BFA washout, Cx26 and Cx43 were localized in the reforming Golgi apparatus (G-I, double arrows; inset in G highlights paranuclear MG160), and by 90 minutes there was diffuse cell surface fluorescence exhibited by Cx26 and Cx43 (J-L, arrow; inset in J reveals paranuclear MG160 localization suggesting a well-organized Golgi apparatus). Also note the prominent population of Cx26 and Cx43 present within the Golgi apparatus (J-L, double arrows). By 2 hours (M-O), Cx26 and Cx43 localization was beginning to resemble control cells. Sparsely cultured cells were used in this experimental set to allow for the connexin distribution patterns to be assessed at sites of cell-cell contact and at free surfaces. Bar, 10 μm.

In order to further examine nascent Cx43 and Cx26 gap junction assembly and translate our findings into living cells and real-time, we first assessed whether the pathways and kinetics of gap junction assembly upon BFA treatment were the same for GFP-tagged Cx43 and Cx26. To this end, BICR-M1R_k cells were engineered to express either Cx43-GFP or Cx26-YFP, and nascent gap junction assembly was re-examined upon BFA washout (Fig. 4). Similarly to untagged Cx43 and Cx26, GFP-tagged connexins were found to clear from the cell surface in the presence of BFA, initially reorganize to the Golgi apparatus upon BFA washout, randomly distribute to the cell surface 1 hour after the removal of BFA, and reach a steady-state distribution pattern similar to that of untreated cells 2 hours after the removal of BFA (Fig. 4I-L). The routing and kinetics for nascent Cx26 and Cx43 assembly into gap junctions were similar to each other and to their untagged connexin counterparts, as presented in Fig. 3. Although fluorescent-protein-tagged connexins were detected at the cell surface approximately 30 minutes earlier than their untagged connexin counterparts, upon the removal of BFA, this may in part reflect an increase in sensitivity of detecting fluorescent-protein-tagged connexins.

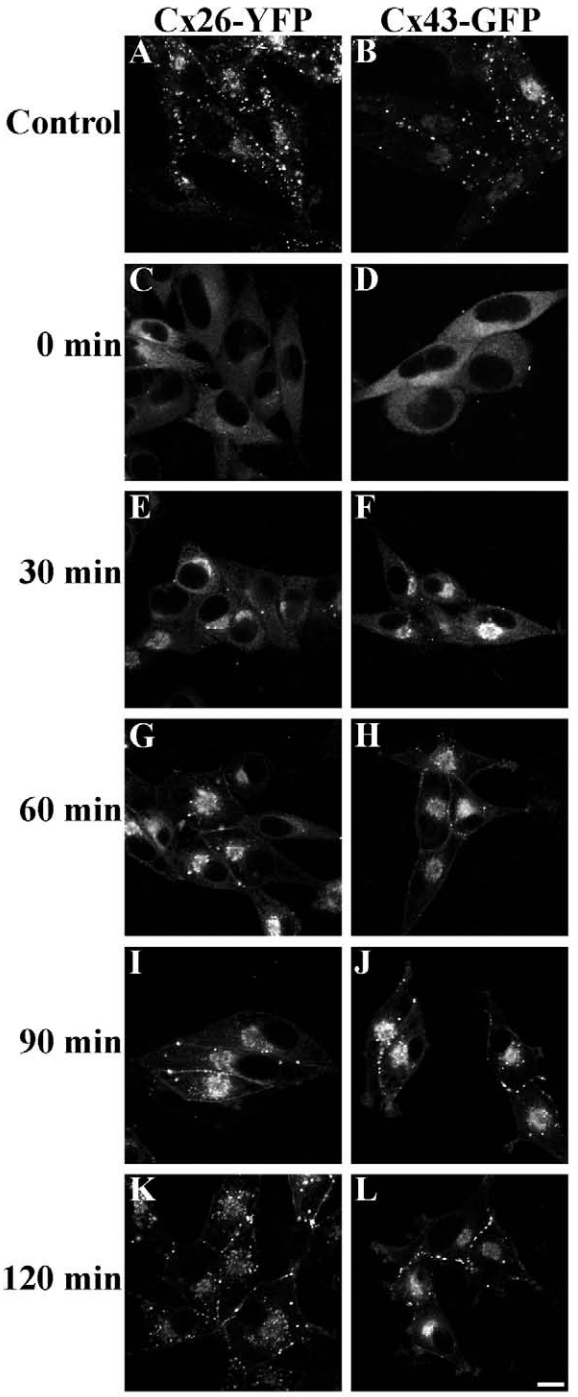

Whereas static imaging allows for partial temporal and spatial localization of connexin during their transport to the plasma membrane, real-time imaging is far more effective for examining active transport processes, including connexin transport carriers. Consequently, continuous time-lapse imaging was performed on BICR-M1R_k cells to assess Cx43 and Cx26 transport and assembly upon different recovery times from BFA pre-treatment. Cx43-GFP (Fig. 5A1,A2 and supplementary material Movie 1) and Cx26-YFP (Fig. 5B1,B2 and supplementary material Movie 2) were observed to move from the ER to the Golgi apparatus within 30 minutes of BFA wash-out. Following the reformation of the Golgi apparatus, Cx43-GFP (Fig. 5C, arrows and supplementary material Movie 3) and Cx26-YFP (Fig. 5D, arrows and supplementary material Movie 4) were found to exit in the form of tubular extensions. Tubular-shaped extensions were highly dynamic, extending and retracting many microns in length from the trans-side of the Golgi apparatus out towards the cell periphery. We found that the Cx43-GFP tubular processes ranged from 3.0 μm to 18.0 μm in length, with a mean length of 6.1±2.8 μm (n=51). Cx26-YFP tubular processes ranged from 3.3 μm to 10.8 μm in length, with a mean length of 5.8±2.2 μm (n=30). Numerous vesicles containing Cx43-GFP (Fig. 5C, arrowheads and supplementary material Movie 3) or Cx26-YFP (Fig. 5D,E, arrowheads and supplementary material Movie 4) were also observed and represented the more common transport intermediate. Ninety minutes after BFA wash-out, diffuse fluorescence was observed at the cell surface (Fig. 5E, double arrows). Time-lapse series supplementary material Movie 5 shows the appearance of bright Cx26-YFP clusters at regions of cell-cell contact and diffused cell surface fluorescence. Similar results were observed at 90 minutes for Cx43-GFP (data not shown). Collectively, these data suggest that connexins are randomly transported to the cell surface and clustering events occur after arrival at sites of cell-cell contact.

Fig. 4. Nascent assembly of fluorescent-protein-tagged Cx26 and Cx43 follow the same kinetics and trafficking routes as untagged connexins. BICR-M1R_k cells stably expressing Cx26-YFP or Cx43-GFP were treated with BFA for 6 hours and fixed at different times after BFA removal. In untreated cells, Cx26-YFP and Cx43-GFP exhibited a paranuclear and cell surface localization pattern (A,B). Both Cx26-YFP and Cx43-GFP were localized within the ER-like compartment at 6 hours of BFA treatment and gap junction plaques were absent (C,D). At 30 minutes post-BFA treatment, both Cx26-YFP and Cx43-GFP were localized to the reformed Golgi apparatus (E,F) and by 60 minutes they were also detected at the cell surface as a diffuse rim of fluorescence (G,H). At 90 minutes, both connexins were visualized as cell surface gap junctions while prominent paranuclear populations of both connexins remained (I,J). Two hours after BFA washout, Cx26-YFP and Cx43-GFP localization resembled that of untreated cells (K,L). Bar, 10 μm.

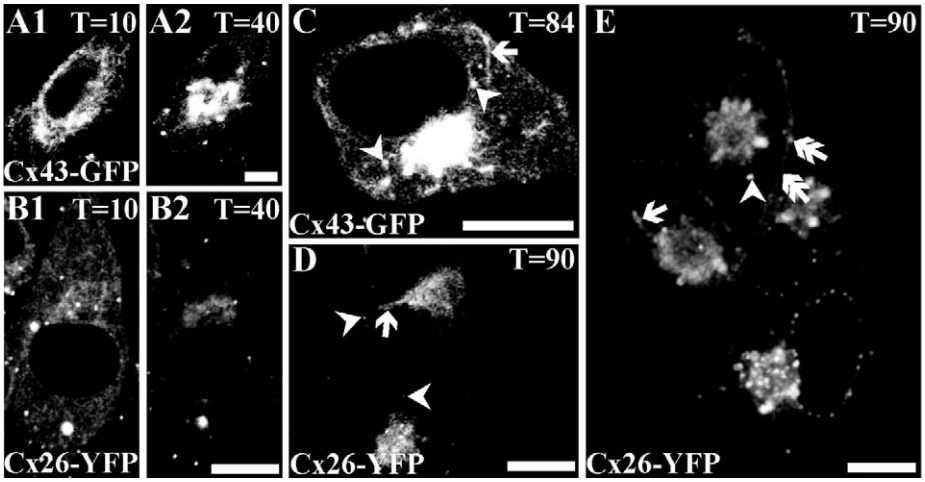

Fig. 5. Cx43-GFP and Cx26-YFP are transported from the Golgi apparatus in both vesicular- and tubular-like PGCs. Time-lapse images of BICR-M1R_k cells expressing Cx43-GFP (A1,A2) or Cx26-YFP (B1,B2) were obtained from 10 to 40 minutes after the removal of BFA. Movies 1 and 2 (see supplementary material) show that both Cx43-GFP and Cx26-YFP were predominantly in the ER initially (T=10) and were transported to paranuclear locations by 40 minutes (T=40), which reflects the re-organization of the Golgi apparatus. Cells imaged (T=84-90 minutes) after BFA removal revealed a paranuclear Golgi-like distribution of Cx43-GFP (C) and Cx26-YFP (D) with subpopulations of tagged connexins emanating from the Golgi in tubular-like structures (C,D, arrows) and vesicular structures (C,D, arrowheads). Tubular extensions and dynamic vesicle movement are best seen in Movies 3 and 4 (see supplementary material). (E) Cx26-YFP could be observed at the cell surface with a diffused rim appearance (double arrow) in cells imaged 90 minutes following BFA-washout. Movie 5 shows vesicles exiting distal elements of the Golgi apparatus and the appearance of bright clusters at cell surface that move rapidly in the plane of the membrane (see supplementary material). Bars, 10 μm.

The disease-linked Cx26 mutant exits the Golgi apparatus

To assess the transport carriers and fate of Cx26 mutants, we expressed a deafness and skin-diseased-linked GFP-tagged Cx26 D66H mutant (Kelsell et al., 2001; Thomas et al., 2004) and a conserved charged variant of this mutation (D66K) (Thomas et al., 2004) in HBL-100 cells. As expected, both mutants were localized to the Golgi apparatus, which was evident by their co-localization with GPP130 (Fig. 6A-F). To assess whether these mutants were capable of actively being delivered to the Golgi apparatus, D66H-GFP was photobleached and a new population of D66H-GFP was recruited to the Golgi apparatus within 60 minutes (Fig. 6G), which suggests that there is dynamic regeneration of this Golgi population of mutant Cx26. Similar results were obtained for D66K-GFP (data not shown). In other time-lapse imaging movies, volatile long tubular extensions containing D66H-GFP were detected (Fig. 6H, arrows), and regional FRAP studies revealed highly dynamic post-Golgi carriers (PGCs) exiting the Golgi apparatus (Fig. 6I, arrows and supplementary material Movie 6). Thus, although the D66H and D66K Cx26 mutants were principally found in the Golgi apparatus, they consistently exit the Golgi apparatus via PGCs in the form of vesicles or tubular extensions. Golgi-exported Cx26 mutants may be targeted to the plasma membrane, where they are unstable and quickly enter a degradation pathway, or retrieved back to the Golgi apparatus. However, we cannot dismiss the possibility that the PGCs containing mutant Cx26 are directly targeted to compartments involved in degradation of mis-folded proteins.

Differential mobility of Cx43 and Cx26 within gap junction plaques

Having examined the characteristics of nascent gap junction formation, we next compared the mobile fraction of Cx43-GFP and Cx26-YFP within gap junction plaques of BICR-M1R_k cells. FRAP analysis in combination with time-lapse imaging revealed that there was a significantly larger mobile fraction ($P<0.05$) in the case of Cx26-YFP when directly compared with Cx43-GFP (Fig. 7A-I). Since channel packing of Cx43 and Cx26 have been reported to be similar (Nunn et al., 2001; Sosinsky, 1996), these results suggest that Cx43 and Cx26 have distinct interactions with connexin-binding proteins that could include cytoskeletal elements. However, it is theoretically possible that the fluorescent protein tags differentially alter the packing density of connexons within gap junction plaques. It is also possible that, during the assembly of gap junctions, punctate fluorescent gap-junction-like structures exist that could be considered formation plaques, which would be expected to exhibit more dynamics owing to the incomplete packing of the channels.

Role of active Cx43 or Cx26 transport from intracellular compartments and microtubules for gap junction plaque regeneration

To investigate whether microtubules plays a differential role in intracellular Cx43 and Cx26 transport, NRK cells expressing fluorescent-protein-tagged Cx43 or Cx26 were first time-lapse imaged prior to nocodazole treatment and then the same field of cells was re-imaged after microtubule depolymerization, as described in Materials and Methods. We previously showed that this treatment condition completely depolymerized microtubules in NRK cells (Thomas et al., 2001). We quantified the movement of vesicles containing fluorescent-protein-tagged Cx43 or Cx26 and found that in both cases there was an ~80% decrease in vesicle movement when microtubules were disrupted (Table 1 and supplementary material Movie 7).

The above experiments suggested that both Cx43-GFP and Cx26-GFP transport are facilitated by intact microtubules. To further investigate the process of steady-state delivery of connexins and their assembly into gap junctions, NRK cells

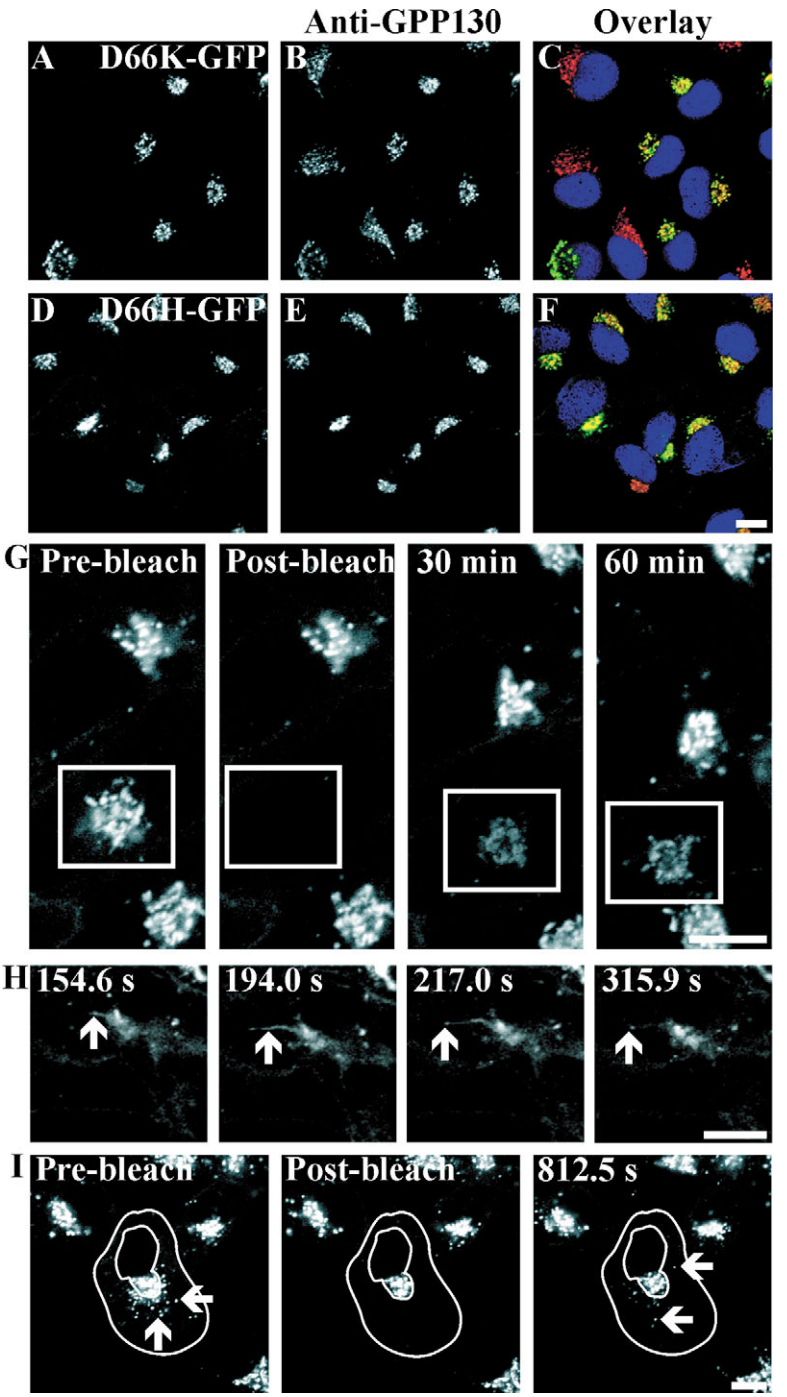

Fig. 6. Golgi-apparatus-localized Cx26 mutants actively exit the Golgi in the form of dynamic tubular extensions and vesicles. HBL-100 cells stably expressing D66K-GFP (A,C, green) or D66H-GFP (D,F, green) were labeled for the cis-Golgi resident protein, GPP130 (B,E,C,F; red). Both D66H-GFP and D66K-GFP exhibit a high degree of co-localization with the Golgi apparatus (C,F, note yellow color). Cells were counterstained with Hoechst 33342 to denote the nuclei (C,F, blue). HBL-100 cells expressing D66H-GFP were time-lapse imaged following photobleaching of the Golgi population (series G, box indicates photobleached region). A new population of D66H-GFP migrated to the photobleached Golgi apparatus with a 40% recovery of fluorescence in 1 hour (based on the pre-bleached area being 100%). Tubular extensions were observed exiting the Golgi apparatus of HBL-100 cells expressing D66H-GFP (series H, arrows). In series I, the area surrounding the Golgi pool of D66K-GFP mutant was photobleached and time-lapse imaged. Highly dynamic vesicles were observed to emanate from the Golgi apparatus within 15 minutes (series I, arrows and supplementary material Movie 6). Bars, 10 μm.

expressing Cx43-GFP or Cx26-GFP were time-lapse imaged during FRAP in the presence of BFA or nocodazole. In the case of Cx26-GFP, a subset of gap junction plaques (Fig. 8A-C) was photobleached in the absence of any treatment (Fig. 8D) or in the presence of the protein transport inhibitor, BFA (Fig. 8E) or the microtubule-disrupter, nocodazole (Fig. 8F). After 1 hour, regenerated Cx26-GFP gap junction plaques were readily observed in control (Fig. 8G) and nocodazole-treated (Fig. 8I) cells but not in BFA-treated cells (Fig. 8H). In control and nocodazole-treated cells, gap junction plaques continued to become more apparent but gap junction regeneration was not evident in BFA-treated cells even after 2 hours (data not shown). Similarly to BFA treatment of cells expressing Cx26-GFP, FRAP analysis of Cx43-GFP gap junctions in NRK cells revealed that the gap junction plaques required continuous Cx43 transport for gap junction regeneration (Fig. 9A-I). In contrast to the findings with Cx26-GFP, however, Cx43-GFP plaque regeneration was inhibited by the disruption of microtubules (Fig. 9C,F,I). It is intriguing that vesicle displacement analysis (Table 1) revealed that fluorescent-protein-tagged Cx43 and Cx26 exhibited approximately the same decrease in the absence of intact microtubules, whereas Cx43-GFP gap junction plaque regeneration was more sensitive to nocodazole than Cx26-GFP. These studies are supported by the previous finding that microtubules are required for enhanced Cx43 gap junction assembly in Novikoff cells and rapid Cx43-GFP vesicle movement in MDCK cells (Johnson et al., 2002).

Discussion

We set out to examine both the delivery of Cx43-GFP and Cx26-YFP to the cell surface under nascent and steady-state conditions, as well as the dynamics and renewal process of gap junctions in living cells. Here we demonstrate that they share similar routing and transport characteristics to each other as well as to their untagged counterparts. Our studies revealed that Cx43-GFP and Cx26-YFP, as well as a disease-linked Cx26 mutant, exited the trans-side of the Golgi apparatus in vesicular and tubular PGCs. Delivery of wild-type connexins to the cell surface appeared random and had no obvious preference for locations of cell-cell contact. Interestingly, movement of Cx26-YFP within a gap junction was more dynamic than Cx43-GFP, which suggests that distinct gap junctions may have different scaffolding properties or interactions with connexin-binding proteins.

Table 1. Microtubule disruption decreases the displacement of intracellular transport vesicles containing Cx26 or Cx43

	Control	10 μM Nocodazole	% Decrease
Cx26	2.18±0.21 μm	0.46±0.05 μm*	78.8
Cx43	2.35±0.39 μm	0.44±0.08 μm*	81.3

NRK cells stably expressing fluorescent-protein-tagged Cx26 or Cx43 were time-lapse imaged before and after nocodazole treatment. Time-lapse movies were used to determine the average connexin-containing vesicle displacement over a period of 1 minute. Movie 7 (see supplementary material) shows the animated time-lapse series corresponding to Cx26-YFP-expressing cells before and after microtubule disruption. *P<0.05.

Cx26 is transported through the Golgi apparatus in NRK and BICR-M1R$_k$ cells

Cx26 and Cx43 have been reported to exhibit unique characteristics that include different intracellular sites of oligomerization. Whereas Cx26 is thought to oligomerize in the endoplasmic reticulum (Falk et al., 1994), substantial evidence suggests that Cx43 assembles into connexons while in the trans-Golgi network (Musil and Goodenough, 1993). Other notable studies using aequorin-tagged Cx26 and connexin-domain substitutions suggest that Cx26 transport to the cell surface is not efficiently blocked by the inhibitor BFA (George et al., 1999; George et al., 1998b) and may not take place through the classical secretory pathway during gap junction biogenesis. This notion was further supported by subcellular fractionation of guinea pig liver tissue, where little Cx26 was found in the Golgi apparatus (Diez et al., 1999). Together with the fact that Cx26 can post-translationally insert into ER membranes in cell-free assays (Ahmad et al., 1999; Zhang et al., 1996) and possibly plasma membranes (Ahmad and Evans, 2002), these results suggest that Cx26 bypasses the Golgi apparatus en route to the cell surface. In the present study, our results using both untagged and fluorescent-protein-tagged Cx26, as well as a disease-linked Cx26 mutant, revealed that a substantial population of Cx26 does indeed pass through the Golgi apparatus. We found in BICR-M1R$_k$ cells that untagged Cx26 and Cx26-YFP were prevented from being transported to the cell surface in the presence of BFA and there was a concomitant loss of gap junction plaques at the cell surface. In addition, expression of wild-type Cx26 in BICR-M1R$_k$ cells resulted in an intracellular population that clearly co-localized with Cx43 in paranuclear regions (reminiscent of the Golgi apparatus) of untreated cells and cells recovering from BFA-treatment. Further confirmation of the essential role of ER-to-Golgi transport of Cx26 was provided by the fact that Sar1-dependent, COPII-mediated ER-to-Golgi transport was required for both Cx26 and Cx43 transport to the plasma membrane. Likewise, FRAP analysis performed in the presence of BFA further demonstrated the necessity of nascent Cx26 delivery to the cell surface from a BFA-sensitive compartment in order to regenerate photobleached Cx26-GFP-containing gap junction plaques. Finally, the retention and retrieval of disease-linked Cx26 mutants to the Golgi apparatus is further evidence that the Golgi apparatus plays a central role in Cx26 secretion. The difference between the present report and former studies may be attributed to cell types examined, or Cx26 may have an alternative route to the plasma membrane when overexpressed. Given the possibility that Cx26 has the capacity to post-translationally import into ER membranes in vitro (Ahmad et al., 1999; Zhang et al., 1996) and possibly directly into plasma membranes (Ahmad and Evans, 2002), it remains possible that a sub-population of Cx26 exhibits diverse routing in the biogenesis of gap junctions. Additionally, there is a growing number of proteins that appear to reach their subcellular destination or the cell surface by a Golgi-independent mechanism, including calsequestrin (Nori et al., 2004), flotillin (Morrow et al., 2002), FGF1 and IL-1α (Prudovsky et al., 2003). Nevertheless our results strongly support the position that, during gap junction biogenesis, a major population of Cx26 proceeds through classical intracellular compartments, including the Golgi apparatus, in a process similar to that previously characterized for Cx43 (Evans et al., 1999; George et al., 1998a; Laird et al., 1995; Musil and Goodenough, 1993; Paulson et al., 2000).

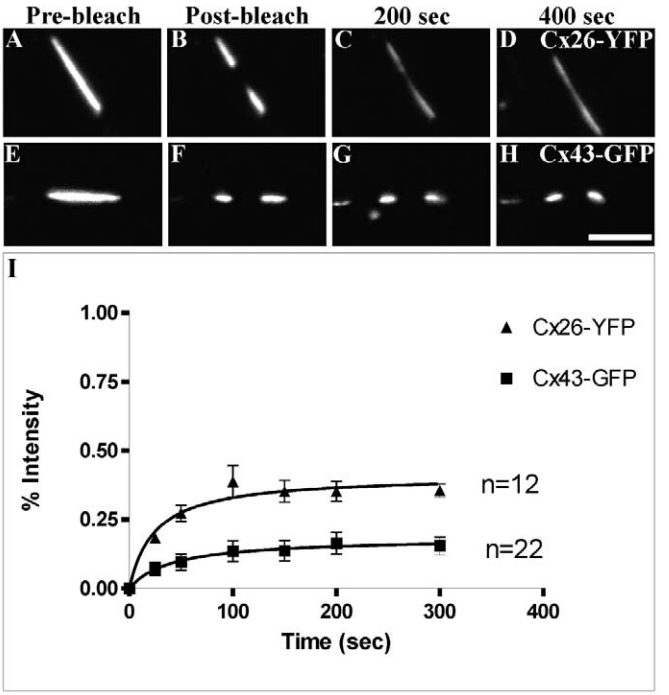

Fig. 7. Differential mobility of fluorescent-protein-tagged Cx26 and Cx43 within assembled gap junctions. Central regions of gap junction plaques in BICR-M1R$_k$ cells, composed of Cx26-YFP (A-D) or Cx43-GFP (E-H), were photobleached and the fluorescent recovery in the photobleached area was monitored. Note the rapid recovery of Cx26-YFP within 200-400 seconds but little recovery was observed in Cx43-GFP photobleached regions of gap junction plaques. Further FRAP analysis revealed that gap junctions composed of Cx26-YFP had a substantially larger mobile fraction population than Cx43-GFP gap junctions (I). Bar, 5 μm.

Delivery of connexins to the plasma membrane

In the present study we used a BFA-treatment and wash-out approach to distinguish between transport intermediates containing connexins that were derived from the Golgi apparatus and delivered to the cell surface from carriers involved in gap junction internalization. We observed the formation of both numerous heterogeneous vesicles and long, labile, tubular extensions derived from the newly reorganized

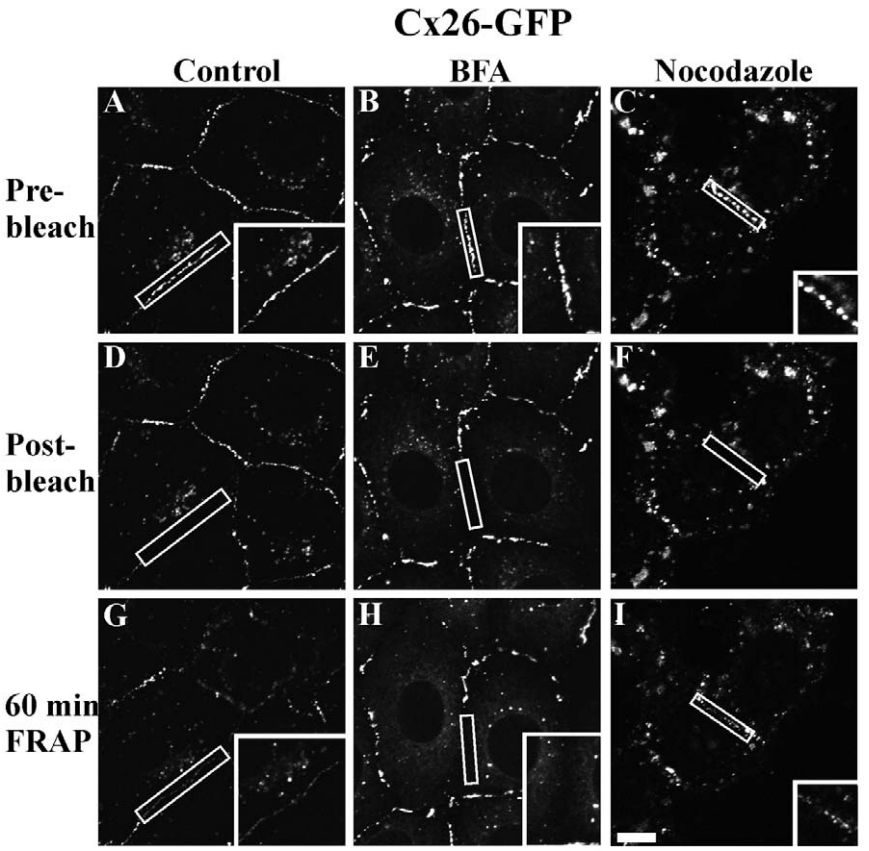

Fig. 8. Steady-state regeneration of Cx26-GFP gap junctions is sensitive to BFA but not nocodazole. NRK cells stably expressing Cx26-GFP were time-lapse imaged following photobleaching of a series of gap junctions (A,D,G, box indicates photobleached area). Cx26-GFP fluorescence steadily recovered within the photobleached area (G, box). ER-to-Golgi transport was disrupted by a 45 minute pre-incubation with BFA followed by FRAP in the presence of BFA (B,E,H, box indicates photobleached area). After 1 hour, there was no detectable Cx26-GFP within the photobleached region of interest (H, box). To disrupt microtubules, nocodazole was added to the cell culture 45 minutes prior to photobleaching of gap junctions in the continued presence of nocodazole (C,F,I). There was significant recovery of Cx26-GFP to the region of interest after 1 hour (I, box), comparable with that occurring under control conditions. Panel inserts represent higher magnifications of the photobleached regions of interest. Experimental sets were repeated seven times with similar results. Bar, 10 μm.

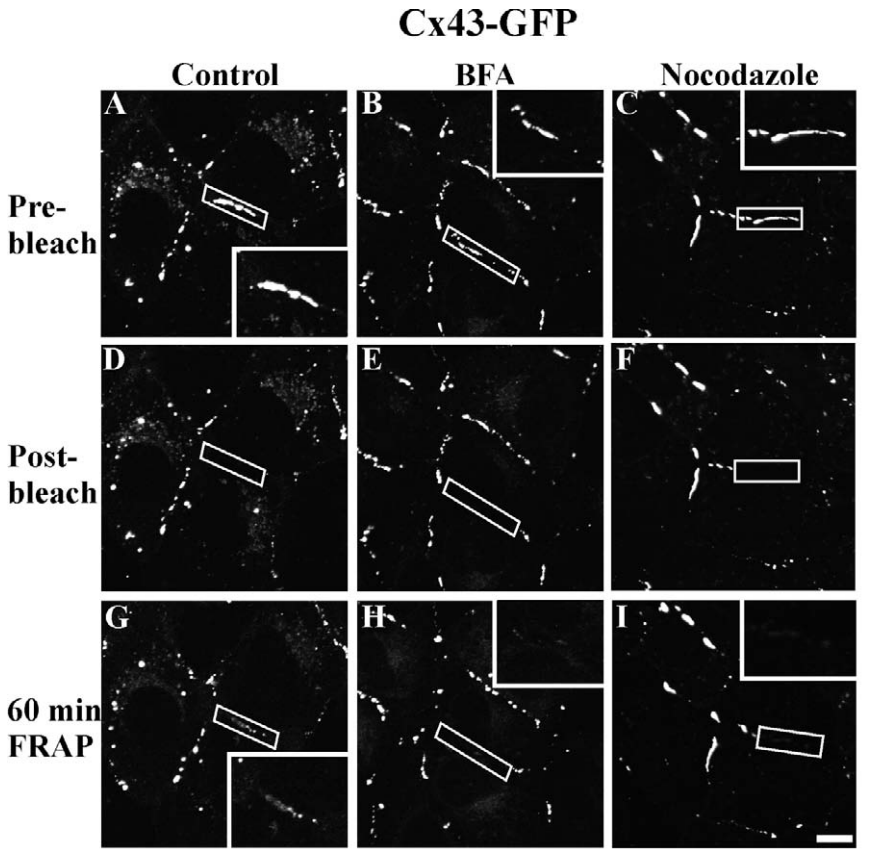

Fig. 9. Steady-state regeneration of Cx43-GFP gap junctions is sensitive to BFA and nocodazole. NRK cells stably expressing Cx43-GFP were time-lapse imaged following photobleaching of a series of gap junctions in the presence of BFA or nocodazole. Control cells revealed substantial recruitment of Cx43-GFP to the photobleached gap junctions after 1 hour (A,D,G) but this level of recovery was not observed in cells treated with BFA (B,E,H) or nocodazole (C,F,I). Panel inserts represent higher magnifications of the photobleached regions of interest. Experimental sets were repeated six times with similar results. Bar, 10 μm.

Golgi apparatus that contained Cx43-GFP or Cx26-YFP. In other studies, tubular PGCs have been shown in other systems to emanate, bifurcate and translocate from the trans-Golgi network as they deliver VSVG-GFP to the plasma membrane (Hirschberg et al., 1998). In this same study it was shown that large pleiomorphic tubular PGCs delivered VSVG-GFP to the cell surface rather than small vesicles. Since we could not identify any direct delivery of connexins via tubular extensions to the plasma membrane, connexin transport within heterogeneous vesicular PGCs may represent the primary transport mechanism for nascent delivery of connexins.

The fusion of PGCs at the cell surface appears to occur randomly at the cell surface of non-polar BICR-M1R$_k$ cells, and some PGCs appear to fuse in close proximity to pre-existing gap junctions and others at free surface where there are no contacting cells. Newly delivered cell surface connexins

appear to cluster laterally within the plane of the membrane with the first stable clustering events occurring preferentially at cell-cell contacts. These findings are consistent with a previously proposed 'selftrap' model (Abney et al., 1987) and the concept of progressive gap junction formation (Johnson et al., 2002; Paulson et al., 2000). Gap junctions grow in size in these 'primed' areas of cell-cell contacts and evidence suggests that gap junction channels are required to be in a clustered state of minimal size in order to function (Bukauskas et al., 2000).

Differential mobility of Cx43-GFP and Cx26-YFP gap junction plaques

Cx43-GFP gap junction plaques in MDCK (Jordan et al., 1999) and RL-CL9 cells (Ingvar Holm, 1999) have been shown to remodel and coalesce in the membrane. Interestingly, in BICR-M1R_k cells we observed that Cx26-YFP gap junctions have a larger mobile fraction in comparison with Cx43-GFP gap junctions. This difference may reflect the possibility that Cx43-GFP intermixing with wild-type Cx43 within the same gap junction plaques would allow for interactions with the scaffolding protein ZO-1 or the microtubule protein β-tubulin, which are known to interact with Cx43 but not Cx26 (Giepmans, 2004; Giepmans and Moolenaar, 1998; Laing et al., 2001). Cx43 gap junction interactions with ZO-1 or β-tubulin may allow for scaffolding with other cytoplasmic proteins, including likely interactions with microfilaments and microtubules. It has been suggested from data obtained from freeze-fracture electron microscopy that cytoskeletal elements were important for the positioning of gap junctions in the membrane (Green and Severs, 1984) and, more recently, Cx43 gap junction channel clustering was shown to be dependent upon intact microfilaments following inhibition of glycosylation (Wang and Rose, 1995). Since Cx26 does not appear to interact with ZO-1 (Kojima et al., 2001), Cx26-YFP gap junctions may exhibit distinctly different anchoring properties and be more subject to lateral flow within the plasma membrane.

Rapid renewal of gap junction plaques

Metabolic labeling and pulse-chase studies have clearly demonstrated that connexins have half-lives of 1.5-3.5 hours (Beardslee et al., 1998; Laing et al., 1997; Laird et al., 1995; Laird et al., 1991) and most studies are consistent with both unassembled connexins and connexins assembled into gap junctions having the same turnover kinetics. Recent studies by Musil and colleagues have shown that a sub-population of connexins is also subject to proteasomal-based turnover in the absence of assembly into gap junctions (VanSlyke et al., 2000; VanSlyke and Musil, 2002). Our earlier studies showing that gap junctions were lost from the cell surface of BICR-M1R_k cells when protein transport was blocked by BFA were consistent with Cx43 gap junctions having the same half-life as monomeric Cx43 (Laird et al., 1995; Laird et al., 1991). In the present study we extended this finding by using FRAP analysis to show that new molecules of Cx43-GFP are recruited into gap junctions with kinetics similar to those suggested by Cx43 pulse-chase studies. More importantly, BFA-treatment studies and FRAP analysis suggest that Cx26-YFP gap junctions have similar turnover kinetics to Cx43-GFP gap junctions. These rapid turnover characteristics provide a mechanism by which gap junctional intercellular communication can be exquisitely regulated in response to physiological stimulus.

We thank Debra Telford for doing the microinjection studies and for assistance in generating the Sar1-DsRed2 vector. This work was supported by Canadian Institute of Health Research grants to D.W.L. and NSERC funding to T.T.

References

Abney, J. R., Braun, J. and Owicki, J. C. (1987). Lateral interactions among membrane proteins. Implications for the organization of gap junctions. *Biophys. J.* **52**, 441-454.

Ahmad, S. and Evans, W. H. (2002). Post-translational integration and oligomerization of connexin 26 in plasma membranes and evidence of formation of membrane pores: implications for the assembly of gap junctions. *Biochem. J.* **365**, 693-699.

Ahmad, S., Diez, J. A., George, C. H. and Evans, W. H. (1999). Synthesis and assembly of connexins in vitro into homomeric and heteromeric functional gap junction hemichannels. *Biochem. J.* **339**, 247-253.

Aridor, M., Bannykh, S. I., Rowe, T. and Balch, W. E. (1995). Sequential coupling between COPII and COPI vesicle coats in endoplasmic reticulum to Golgi transport. *J. Cell Biol.* **131**, 875-893.

Bakirtzis, G., Jamieson, S., Aasen, T., Bryson, S., Forrow, S., Tetley, L., Finbow, M., Greenhalgh, D. and Hodgins, M. (2003). The effects of a mutant connexin 26 on epidermal differentiation. *Cell Commun. Adhes.* **10**, 359-364.

Beardslee, M. A., Laing, J. G., Beyer, E. C. and Saffitz, J. E. (1998). Rapid turnover of connexin43 in the adult rat heart. *Circul. Res.* **83**, 629-635.

Bukauskas, F. F., Jordan, K., Bukauskiene, A., Bennett, M. V., Lampe, P. D., Laird, D. W. and Verselis, V. K. (2000). Clustering of connexin 43-enhanced green fluorescent protein gap junction channels and functional coupling in living cells. *Proc. Natl. Acad. Sci. USA* **97**, 2556-2561.

Dascher, C. and Balch, W. E. (1994). Dominant inhibitory mutants of ARF1 block endoplasmic reticulum to Golgi transport and trigger disassembly of the Golgi apparatus. *J. Biol. Chem.* **269**, 1437-1448.

Diez, J. A., Ahmad, S. and Evans, W. H. (1999). Assembly of heteromeric connexons in guinea-pig liver en route to the Golgi apparatus, plasma membrane and gap junctions. *Eur. J. Biochem.* **262**, 142-148.

Evans, W. H., Ahmad, S., Diez, J., George, C. H., Kendall, J. M. and Martin, P. E. (1999). Trafficking pathways leading to the formation of gap junctions. *Novartis Foun. Symp.* **219**, 44-54.

Falk, M. M. (2000). Connexin-specific distribution within gap junctions revealed in living cells. *J. Cell Sci.* **113**, 4109-4120.

Falk, M. M. and Gilula, N. B. (1998). Connexin membrane protein biosynthesis is influenced by polypeptide positioning within the translocon and signal peptidase access. *J. Biol. Chem.* **273**, 7856-7864.

Falk, M. M., Kumar, N. M. and Gilula, N. B. (1994). Membrane insertion of gap junction connexins: polytopic channel forming membrane proteins. *J. Cell Biol.* **127**, 343-355.

Falk, M. M., Buehler, L. K., Kumar, N. M. and Gilula, N. B. (1997). Cell-free synthesis and assembly of connexins into functional gap junction membrane channels. *EMBO J.* **16**, 2703-2716.

Forge, A., Marziano, N. K., Casalotti, S. O., Becker, D. L. and Jagger, D. (2003). The inner ear contains heteromeric channels composed of cx26 and cx30 and deafness-related mutations in cx26 have a dominant negative effect on cx30. *Cell. Commun. Adhes.* **10**, 341-346.

Galipeau, J., Li, H., Paquin, A., Sicilia, F., Karpati, G. and Nalbantoglu, J. (1999). Vesicular Stomatis Virus G pseudotyped retrovector mediates effective in vivo suicide gene delivery in experimental brain cancer. *Cancer Res.* **59**, 2384-2394.

Gemel, J., Valiunas, V., Brink, P. R. and Beyer, E. C. (2004). Connexin43 and connexin26 form gap junctions, but not heteromeric channels in co-expressing cells. *J. Cell Sci.* **117**, 2469-2480.

George, C. H., Kendall, J. M., Campbell, A. K. and Evans, W. H. (1998a). Connexin-aequorin chimerae report cytoplasmic calcium environments along trafficking pathways leading to gap junction biogenesis in living COS-7 cells. *J. Biol. Chem.* **273**, 29822-29829.

George, C. H., Martin, P. E. and Evans, W. H. (1998b). Rapid determination of gap junction formation using HeLa cells microinjected with cDNAs

encoding wild-type and chimeric connexins. *Biochem. Biophys. Res. Commun.* **247**, 785-789.

George, C. H., Kendall, J. M. and Evans, W. H. (1999). Intracellular trafficking pathways in the assembly of connexins into gap junctions. *J. Biol. Chem.* **274**, 8678-8685.

Giepmans, B. N. (2004). Gap junctions and connexin-interacting proteins. *Cardiovasc. Res.* **62**, 233-245.

Giepmans, B. N. and Moolenaar, W. H. (1998). The gap junction protein connexin43 interacts with the second PDZ domain of the zona occludens-1 protein. *Curr. Biol.* **8**, 931-934.

Gonatas, J. O., Mezitis, S. G. E., Stieber, A., Fleischer, B. and Gonatas, N. K. (1989). MG-160: A novel sialoglycoprotein of the medial cisternae of the Golgi apparatus. *J. Biol. Chem.* **264**, 646-653.

Green, C. R. and Severs, N. J. (1984). Connexon rearrangement in cardiac gap junctions: evidence for cytoskeletal control? *Cell Tissue Res.* **237**, 185-186.

Haucke, V. (2003). Vesicle budding: a coat for the COPs. *Trends Cell Biol.* **13**, 59-60.

Hirschberg, K., Miller, C. M., Ellenberg, J., Presley, J. F., Siggia, E. D., Phair, R. D. and Lippincott-Schwartz, J. (1998). Kinetic analysis of secretory protein traffic and characterization of Golgi to plasma membrane transport intermediates in living cells. *J. Cell Biol.* **143**, 1485-1503.

Holm, I., Mikhailov, A., Jillson, T. and Rose, B. (1999). Dynamics of gap junctions observed in living cells with connexin43-GFP chimeric protein. *Eur. J. Cell Biol.* **78**, 856-866.

Johnson, R. G., Meyer, R. A., Li, X. R., Preus, D. M., Tan, L., Grunenwald, H., Paulson, A. F., Laird, D. W. and Sheridan, J. D. (2002). Gap junctions assemble in the presence of cytoskeletal inhibitors, but enhanced assembly requires microtubules. *Exp. Cell Res.* **275**, 67-80.

Jordan, K., Solan, J. L., Dominguez, M., Sia, M., Hand, A., Lampe, P. D. and Laird, D. W. (1999). Trafficking, assembly, and function of a connexin43-green fluorescent protein chimera in live mammalian cells. *Mol. Biol. Cell* **10**, 2033-2050.

Kelsell, D. P., Di, W. L. and Houseman, M. J. (2001). Connexin mutations in skin disease and hearing loss. *Am. J. Hum. Genet.* **68**, 559-568.

Kojima, T., Kokai, Y., Chiba, H., Yamamoto, M., Mochizuki, Y. and Sawada, N. (2001). Cx32 but not Cx26 is associated with tight junctions in primary cultures of rat hepatocytes. *Exp. Cell Res.* **263**, 193-201.

Koval, M., Harley, J. E., Hick, E. and Steinberg, T. H. (1997). Connexin46 is retained as monomers in a trans-Golgi compartment of osteoblastic cells. *J. Cell Biol.* **137**, 847-857.

Laing, J. G., Tadros, P. N., Westphale, E. M. and Beyer, E. C. (1997). Degradation of connexin43 gap junctions involves both the proteasome and the lysosome. *Exp. Cell Res.* **236**, 482-492.

Laing, J. G., Manley-Markowski, R. N., Koval, M., Civitelli, R. and Steinberg, T. H. (2001). Connexin45 interacts with zonula occludens-1 and connexin43 in osteoblastic cells. *J. Biol. Chem.* **276**, 23051-23055.

Laird, D. W., Puranam, K. L. and Revel, J. P. (1991). Turnover and phosphorylation dynamics of connexin43 gap junction protein in cultured cardiac myocytes. *Biochem. J.* **273**, 67-72.

Laird, D. W., Castillo, M. and Kasprzak, L. (1995). Gap junction turnover, intracellular trafficking, and phosphorylation of connexin43 in brefeldin A-treated rat mammary tumor cells. *J. Cell Biol.* **131**, 1193-1203.

Laird, D. W., Jordan, K. and Shao, Q. (2001). Expression and imaging of connexin-GFP chimeras in live mammalian cells. *Methods Mol. Biol.* **154**, 135-142.

Lippincott-Schwartz, J., Snapp, E. and Kenworthy, A. (2001). Studying protein dynamics in living cells. *Mol. Cell. Biol.* **2**, 444-455.

Mao, A. J., Bechberger, J., Lidington, D., Galipeau, J., Laird, D. W. and Naus, C. C. (2000). Neuronal differentiation and growth control of neuro-2a cells after retroviral gene delivery of connexin43. *J. Biol. Chem.* **275**, 34407-34414.

Martin, P. E., Errington, R. J. and Evans, W. H. (2001). Gap junction assembly: multiple connexin fluorophores identify complex trafficking pathways. *Cell Commun. Adhes.* **8**, 243-248.

Marziano, N. K., Casalotti, S. O., Portelli, A. E., Becker, D. L. and Forge, A. (2003). Mutations in the gene for connexin 26 (GJB2) that cause hearing loss have a dominant negative effect on connexin 30. *Hum. Mol. Genet.* **12**, 805-812.

Morrow, I. C., Rea, S., Martin, S., Prior, I. A., Prohaska, R., Hancock, J. F., James, D. E. and Parton, R. G. (2002). Flotillin-1/reggie-2 traffics to surface raft domains via a novel Golgi-independent pathway. Identification of a novel membrane targeting domain and a role for palmitoylation. *J. Biol. Chem.* **277**, 48834-48841.

Musil, L. S. and Goodenough, D. A. (1993). Multisubunit assembly of an integral plasma membrane channel protein, gap junction connexin43, occurs after exit from the ER. *Cell* **74**, 1065-1077.

Nori, A., Bortoloso, E., Frasson, F., Valle, G. and Volpe, P. (2004). Vesicle budding from endoplasmic reticulum is involved in calsequestrin routing to sarcoplasmic reticulum of skeletal muscles. *Biochem. J.* **379**, 505-512.

Nunn, R. S., Macke, T. J., Olson, A. J. and Yeager, M. (2001). Transmembrane alpha-helices in the gap junction membrane channel: systematic search of packing models based on the pair potential function. *Microsc. Res. Tech.* **52**, 344-351.

Paulson, A. F., Lampe, P. D., Meyer, R. A., TenBroek, E., Atkinson, M. M., Walseth, T. F. and Johnson, R. G. (2000). Cyclic AMP and LDL trigger a rapid enhancement in gap junction assembly through a stimulation of connexin trafficking. *J. Cell Sci.* **113**, 3037-3049.

Paznekas, W. A., Boyadjiev, S. A., Shapiro, R. E., Daniels, O., Wollnik, B., Keegan, C. E., Innis, J. W., Dinulos, M. B., Christian, C., Hannibal, M. C. et al. (2003). Connexin 43 (GJA1) mutations cause the pleiotropic phenotype of oculodentodigital dysplasia. *Am. J. Hum. Genet.* **72**, 408-418.

Prudovsky, I., Mandinova, A., Soldi, R., Bagala, C., Graziani, I., Landriscina, M., Tarantini, F., Duarte, M., Bellum, S., Doherty, H. et al. (2003). The non-classical export routes: FGF1 and IL-1alpha point the way. *J. Cell Sci.* **116**, 4871-4881.

Qin, H., Shao, Q., Belliveau, D. J. and Laird, D. W. (2001). Aggregated DsRed-tagged Cx43 and over-expressed Cx43 are targeted to lysosomes in human breast cancer cells. *Cell Commun. Adhes.* **8**, 433-439.

Qin, H., Shao, Q., Curtis, H., Galipeau, J., Belliveau, D. J., Wang, T., Alaoui-Jamali, M. A. and Laird, D. W. (2002). Retroviral delivery of connexin genes to human breast tumor cells inhibits in vivo tumor growth by a mechanism that is independent of significant gap junctional intercellular communication. *J. Biol. Chem.* **277**, 29132-29138.

Richardson, R., Donnai, D., Meire, F. and Dixon, M. J. (2004). Expression of Gja1 correlates with the phenotype observed in oculodentodigital syndrome/type III syndactyly. *J. Med. Genet.* **41**, 60-67.

Rouan, F., White, T. W., Brown, N., Taylor, A. M., Lucke, T. W., Paul, D. L., Munro, C. S., Uitto, J., Hodgins, M. B. and Richard, G. (2001). trans-dominant inhibition of connexin-43 by mutant connexin-26: implications for dominant connexin disorders affecting epidermal differentiation. *J. Cell Sci.* **114**, 2105-2113.

Saez, J. C., Berthoud, V. M., Branes, M. C., Martinez, A. D. and Beyer, E. C. (2003). Plasma membrane channels formed by connexins: their regulation and functions. *Physiol. Rev.* **83**, 1359-1400.

Sosinsky, G. E. (1996). Molecular organization of gap junction membrane channels. *J. Bioenerg. Biomembr.* **28**, 297-309.

Thomas, T., Jordan, K. and Laird, D. W. (2001). Role of cytoskeletal elements in the recruitment of Cx43-GFP and Cx26-YFP into gap junctions. *Cell Commun. Adhes.* **8**, 231-236.

Thomas, T., Telford, D. and Laird, D. W. (2004). Functional domain mapping and selective trans-dominant effects exhibited by Cx26 disease-causing mutations. *J. Biol. Chem.* **279**, 19157-19168.

VanSlyke, J. K. and Musil, L. S. (2002). Dislocation and degradation from the ER are regulated by cytosolic stress. *J. Cell Biol.* **157**, 381-394.

VanSlyke, J. K., Deschenes, S. M. and Musil, L. S. (2000). Intracellular transport, assembly, and degradation of wild-type and disease-linked mutant gap junction proteins. *Mol. Biol. Cell* **11**, 1933-1946.

Wang, Y. and Rose, B. (1995). Clustering of Cx43 cell-to-cell channels into gap junction plaques: regulation by cAMP and microfilaments. *J. Cell Sci.* **108**, 3501-3508.

Willecke, K., Eiberger, J., Degen, J., Eckardt, D., Romualdi, A., Guldenagel, M., Deutsch, U. and Sohl, G. (2002). Structural and functional diversity of connexin genes in the mouse and human genome. *Biol. Chem.* **383**, 725-737.

Zhang, J. T., Chen, M., Foote, C. I. and Nicholson, B. J. (1996). Membrane integration of in vitro-translated gap junctional proteins: co- and post-translational mechanisms. *Mol. Biol. Cell* **7**, 471-482.